PHYSICAL REVIEW E **92**, 021002(R) (2015)

Jet drops from bursting bubbles: How gravity and viscosity couple to inhibit droplet production

Peter L. L. Walls,[1] Louis Henaux,[1,2] and James C. Bird[1,*]
[1]*Department of Mechanical Engineering, Boston University, Boston, Massachusetts 02215, USA*
[2]*École Polytechnique, Route de Saclay, 91128 Palaiseau, France*
(Received 30 April 2015; published 17 August 2015)

When a bubble ruptures at a liquid surface the collapsing cavity produces a central jet that frequently breaks up into a series of droplets. Current experiment and theory predict that the production of jet drops will be limited by either viscous or gravitational effects. However, while there are a number of studies focusing on these two limiting cases, less is understood about the production of jet drops when both gravitational and viscous effects are significant. Here, we uncover the existence of an intermediate region where both gravitational and viscous effects play a critical role in jet-drop formation. We propose that the role of gravity is most important before rupture, and carry out simulations that demonstrate the importance of the equilibrium bubble shape in the production of jet drops.

DOI: 10.1103/PhysRevE.92.021002 PACS number(s): 47.55.D−, 47.15.Uv, 47.35.Pq, 92.60.Mt

Droplet production from bursting bubbles is ubiquitous and has been studied for over 80 years owing to its importance in fields ranging from disease transfer [1–5] to earth science [6–10]. Over the ocean, it has been estimated that between 10^{18} and 10^{20} bubbles burst per second [11]. The droplets produced by these bubbles are a significant source of particulates, such as sea salt, in the atmosphere [9–11]. Similarly over land, the aroma that often accompanies rainfall has been linked to chemicals in droplets aerosolized by small bubbles bursting on a rain droplet's surface [12,13]. Whenever a bubble ruptures there are two mechanisms for droplet formation: the retracting thin film can fragment into film drops [14–16] and the column of water rising from the center can break up into jet droplets [17–23]. Our paper examines the conditions necessary for a jet droplet to be produced.

The jetting phenomenon is illustrated in Fig. 1. Here, we have injected air into the bottom of a water-glycerol solution with known viscosity μ_ℓ, density ρ_ℓ, and surface tension γ. The air bubble rises to the surface and establishes an equilibrium shape with cap radius R. We film the spontaneous rupture of the bubble and subsequent jetting phenomenon with a high-speed camera at frame rates ranging from 50 000 to 100 000 frames per second. In the first moments after rupture, capillary waves travel down the side of the bubble, and upon colliding create a region of high curvature at the bottom of the bubble [11,19]. The capillary pressure associated with this curvature creates an upward swell, or jet, of liquid [24]. Under certain conditions, the jet will break up into one or more jet drops [Fig. 1(a)]. Under other conditions, a jet may form, but does not emit a droplet before returning to the interface [Fig. 1(b)].

For a jet drop to form, the size of the bubbles needs to lie in a certain range. Previous studies show that under conditions in which the Ohnesorge number, $\mathrm{Oh} \equiv \mu_\ell/\sqrt{\rho_\ell \gamma R}$, exceeds a critical value $\mathrm{Oh_c} \approx 0.037$, jet drops are not produced because the inertial capillary waves driving the motion are damped out by viscous stresses [20,26]. Similarly, under conditions in which the Bond number, $\mathrm{Bo} \equiv \rho_\ell g R^2/\gamma$ exceeds a critical value $\mathrm{Bo_c} \approx 3$, jet drops are not produced because of the influence of gravity on the equilibrium bubble shape and on the upward motion of the jet [27]. Thus, we expect air bubbles in water to produce jet droplets when the size (cap radius) is between $R = 8$ μm ($\mathrm{Oh} < \mathrm{Oh_c}$) and $R = 4.2$ mm ($\mathrm{Bo} < \mathrm{Bo_c}$). Since jet drops were not observed in Fig. 1(b), it is tempting to assume that either gravity or viscosity is preventing droplet formation; yet both $\mathrm{Oh} < \mathrm{Oh_c}$ and $\mathrm{Bo} < \mathrm{Bo_c}$ are well within the jet-drop regime. Therefore, relying on current theory, it is not immediately obvious why droplets are absent in Fig. 1(b).

To explore the extent of this phenomenon, we carry out a series of experiments in which we systematically vary the bubble size R and range of the liquid viscosity μ_ℓ. We control the viscosity, measured with a vibrating-plate viscometer [28], over an order of magnitude by adjusting the weight percentage of glycerol in a water bath (Table I). Surface tension, measured by the pendant drop method [29], and density also vary with glycerol concentration, but to a significantly smaller degree than viscosity. It is important to note that for a bubble to form a stable equilibrium shape, surfactants resulting in marginal regeneration must be present [16]. These naturally occurring surfactants, adsorbed onto the liquid interface from the surroundings, tend to produce a surface pressure of $\Delta\gamma \sim 1$ mN m^{-1}. In fact, even a minuscule amount of natural surfactant is sufficient to prevent bubbles from rupturing immediately upon reaching the free surface. Indeed, comparing our value of surface tension for pure water ($\gamma = 70$ mN m^{-1}) with tabulated values ($\gamma = 72$ mN m^{-1}) we see that the expected surface pressure is consistent with our measured values [30].

Figure 2(a) depicts the size R and viscosity μ_ℓ of each bubble used in our experiments. The dash-dotted lines denoting the critical $\mathrm{Oh_c}$ and $\mathrm{Bo_c}$ numbers [Fig. 2(a)] are calculated using the average liquid properties (Table I). As expected, bubbles do not produce jet drops (closed symbols) within either region exceeding the critical values [shaded regions in Fig. 2(a)]. However, while points A and B [corresponding to Figs. 1(a) and 1(b)] fall within the region of droplet production (unshaded region), only A produces droplets (open symbols). In fact, we find that a number of our experiments falling inside the unshaded region do not produce any droplets; a result that contradicts our expectation. Replotting our data in dimensionless terms (Bo and Oh) reveals an intermediate

*Corresponding author: jbird@bu.edu

 ©2015 American Physical Society

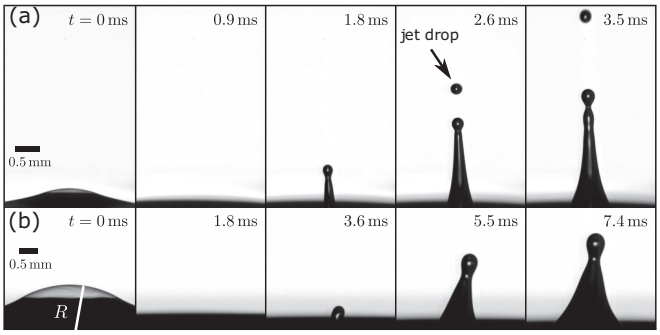

FIG. 1. High-speed series of images showing the evolution of two rupturing air bubbles in glycerol-water mixtures. (a) Under certain conditions (cap radius of curvature $R = 1.7$ mm, viscosity $\mu_\ell = 3.5$ mPa s) a central jet rises and produces one or more jet droplets. (b) Under other conditions ($R = 2.7$ mm, $\mu_\ell = 9.9$ mPa s), a central jet rises but no droplets are produced. The absence of jetting in this case cannot be explained by gravitational or viscous effects alone (see Supplemental Material videos [25]).

region wherein the limit on droplet production is not solely determined by either the value of Bond or Ohnesorge number [Fig. 2(b)]. Instead, our experimental data suggests that viscosity and gravity couple in this region preventing droplet production earlier than anticipated. To test this hypothesis, we turn to simulation.

We model a collapsing bubble using conservation of mass and momentum, assuming an incompressible flow for both the liquid and gas phases. Our approach is to use a volume-of-fluid (VOF) method solving for both phases simultaneously while varying density and viscosity smoothly across the interface, which has a constant surface tension [31]. To develop the model, we rescale the two-phase Navier-Stokes equations by the cap radius R and the inertio-capillary time scale $\sqrt{\rho_\ell R^3/\gamma}$. With these scalings, the effects of gravity and viscosity are quantified solely by the Bo and Oh numbers [32]. While surface tension gradients and boundary effects are present in our experiments, we focus on the effects of viscosity and gravity by removing the thin film cap and modeling the remaining cavity in a large domain ($16R \times 16R$) to minimize the influence of the container. To solve our proposed model we utilize the open source flow solver Gerris [33,34]. We choose to numerically solve the model using Gerris because of its proven accuracy in surface tension driven problems and ability to adaptively mesh over nearly five orders of magnitude in spatial scale [35–37].

TABLE I. Measured values of density ρ_ℓ, dynamic viscosity μ_ℓ, and surface tension γ for the various water-glycerol solutions used in our experiments.

	□,■	○,●	△,▲	▽,▼	◆	⬟
Glycerol wt %	0	40	52	60	65	70
$\rho_\ell\,(\mathrm{kg\,m^{-3}})$	997	1100	1130	1150	1170	1180
$\mu_\ell\,(\mathrm{mPa\,s})$	0.9	3.5	5.8	9.9	13.5	20.3
$\gamma\,(\mathrm{mN\,m^{-1}})$	70	67	66	64	63	63

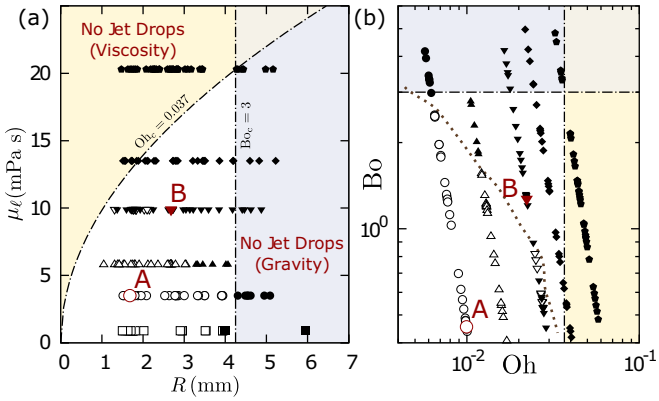

FIG. 2. (Color online) Compilation of individual bubble bursting experiments that lead to jet drops (open symbols) and no jet drops (closed symbols). The regimes in which viscosity or gravity alone would prevent jet drops from forming are indicated with shading. (a) Jet drops are expected only for a certain range of bubble sizes (as measured by cap radius R), and this range decreases as the viscosity increases (unshaded region). Yet, jet drops are not observed in much of this region. Here, the symbols indicate the particular liquid represented by the same symbol in Table I. (b) The experimental data is replotted in terms of the Ohnesorge number, $\mathrm{Oh} = \mu_\ell/\sqrt{\rho_\ell \gamma R}$, and the Bond number, $\mathrm{Bo} = \rho_\ell g R^2/\gamma$, on a logarithmic scale. The dotted line is a guide for the eye separating the observation of droplets from no droplets. The dash-dotted lines denoting the critical $\mathrm{Bo_c}$ and $\mathrm{Oh_c}$ are calculated using the average property values in Table I.

The simulation results corresponding to our two initial experiments (Fig. 1) are shown in Fig. 3. The evolution of the collapse is shown at the dimensionless times ($\tau = t/\sqrt{\rho_\ell R^3/\gamma}$) corresponding to the time of each image in Fig. 1. Our simulations predict both the production of jet droplets [Fig. 3(a)] and the phenomenon of no droplets being produced in the intermediate region [Fig. 3(b)], consistent with our observations (Fig. 1). Therefore it appears that the lack of jet drops in our experiments is not a consequence of boundary

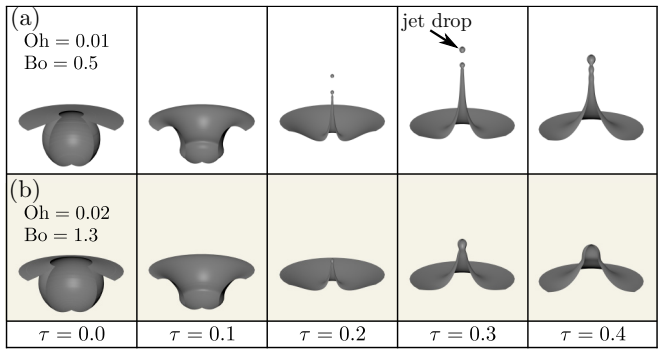

FIG. 3. (Color online) A series of simulation results matching the experimental series shown in Fig. 1. Each series is matched by the Bond and Ohnesorge numbers aligned with the inertio-capillary time $\tau = t/\sqrt{\rho_\ell R^3/\gamma}$. (a) The simulations predict that a jet drop forms when $\mathrm{Oh} = 0.01$, $\mathrm{Bo} = 0.5$, as expected. (b) The simulations predict that no jet drops are formed when $\mathrm{Oh} = 0.02$, $\mathrm{Bo} = 1.3$, consistent with our experiments.

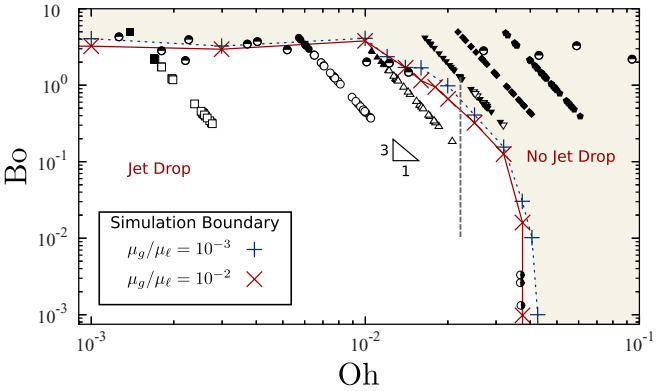

FIG. 4. (Color online) Simulation boundary of jet droplet production illustrating the extent of the intermediate region where gravity and viscosity are significant. The surrounding gas has a minimal influence in determining the limits on droplet formation in the viscosity ratio range $\mu_g/\mu_\ell = 10^{-3}$ to 10^{-2}. The predicted boundaries are in agreement with both our experimental results [data from Fig. 2(a)] and those results of previous studies [Bond (๏) [27] and Ohnesorge (๏) [26]]. The vertical dotted line at Oh = 0.02 indicates the location of the simulations used to investigate the role of gravity in the jetting process (Fig. 5).

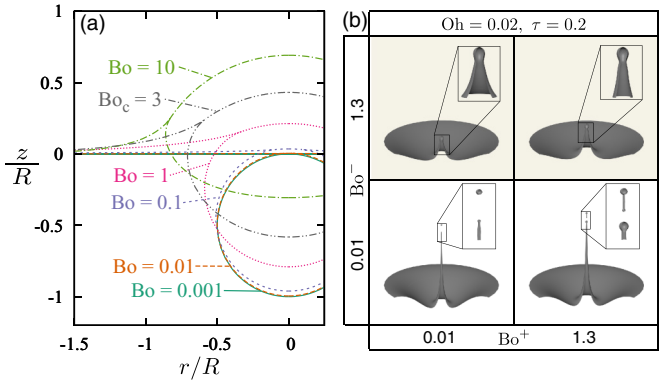

FIG. 5. (Color online) Results of a series of simulations designed to probe the role of gravity in the production of jet droplets. The effects of Bond number (gravity) in the jetting process are divided into those occurring before (Bo^-) and after (Bo^+) the bubble bursts. (a) The shape of a bubble in equilibrium is uniquely determined by the value of Bo^-, tending to flatten out as gravity becomes increasingly important. (b) When $Bo^- = Bo^+$, the result is equivalent to experimental observation (vertical dashed line in Fig. 4). The simulations show that a 100× increase in $Bo^+ = 0.01 \rightarrow 1.3$ for the $Bo^- = 0.01$ case has little effect on droplet production. Likewise, a 100× decrease in $Bo^+ = 1.3 \rightarrow 0.01$ for the $Bo^- = 1.3$ case does not encourage jet droplets to form. Yet, a change in Bo^- (the shape of the bubble) completely accounts for the change in jet production.

effects or surfactant gradients, and instead can be rationalized solely by a combination of gravitational and viscous effects.

We perform a series of simulations extending the previously determined boundaries for droplet production into a continuous boundary valid for all combinations of Bond and Ohnesorge numbers. Figure 4 illustrates that we recover the existing constant value limits on the Ohnesorge (๏) [26] and Bond (๏) [27] numbers when gravity and viscosity can be neglected, respectively. To account for the variation in the viscosity ratios in our experiments, we calculate the boundary for $\mu_g/\mu_\ell = 10^{-3}$ and 10^{-2}, where μ_g is the viscosity of the gas phase. We see that this order of magnitude change in the viscosity ratio has a minimal effect on the location of the boundary for jet droplet production (Fig. 4). Moreover, the numerically predicted intermediate region follows an approximate power law $\mathrm{Bo} \propto \mathrm{Oh}^{-3}$ and aligns well with our experimental data from Fig. 2.

It is unsurprising that the previous works investigating the limits of droplet production did not observe this region. In the numerical work concerning the upper size limit, $\mathrm{Bo} \approx 3.0$ (๏), viscosity is largely neglected in the modeling [27]. Similarly, the experimental work concerning the lower size limit, $\mathrm{Oh} \approx 0.037$ (๏), was conducted in an area in which $\mathrm{Bo} \ll 1$ [26]. Indeed, Fig. 4 confirms that neglecting the effects of gravity is justified when $\mathrm{Bo} \lesssim 0.01$.

To understand why gravity influences the viscous limit on jet droplet production when $\mathrm{Bo} \gtrsim 0.01$, we decouple the effects of the Bond number to before and after bubble rupture. Before rupture, the Bond number determines the equilibrium shape for the bubble at the free surface [38]. Equilibrium shapes normalized by the cap radius R are shown for several values of Bond number in Fig. 5(a). As the Bond number increases, the equilibrium shape transitions from a spherical bubble ($\mathrm{Bo} \rightarrow 0$) to a hemispherical cap ($\mathrm{Bo} \rightarrow \infty$). After rupture, the Bond number determines the magnitude of the deceleration acting on the rising liquid jet. For larger bubbles, the resulting jet typically experiences a larger decelerating force from gravity than smaller bubbles experience as the jet contains a larger mass of liquid and hence a larger weight. Regardless of which effect is dominating the dynamics, we have found that it becomes insignificant when $\mathrm{Bo} \lesssim 0.01$ (Fig. 4). It is worth noting that $\mathrm{Bo} = 0.01$ and $\mathrm{Bo} = 0.001$ are indistinguishable on the scale of the cap radius R [Fig. 5(a)], leading us to hypothesize that the dominant role of gravity in jet-drop formation is setting up the bubble shape.

To test if the transition to the intermediate region can be understood in terms of the bubble shape alone, we perform a series of simulations in which we independently adjust the Bond number before (Bo^-) and after (Bo^+) the bubble ruptures. Specifically, the value of Bo^- determines the initial bubble shape [Fig. 5(a)] and Bo^+ determines the relative strength of gravity in the subsequent jetting. We first begin with the initial nondroplet producing case shown in Figs. 1(b) and 3(b) ($\mathrm{Oh} = 0.02$, $\mathrm{Bo} = 1.3$). In this simulation [Fig. 5(b), top right], the Bond numbers before and after rupture are set equal to represent the experimental conditions ($Bo^- = Bo^+ = 1.3$). The liquid jet rises vertically without pinching off, here shown at the dimensionless time where droplets are typically observed [$\tau = 0.2$, 3.6 ms in Fig. 1(b)]. We next reduce both Bond numbers to 0.01 while holding the Ohnesorge number constant at 0.02 (vertical dotted line in Fig. 4). As expected from Fig. 4, jet drops are produced under these conditions [Fig. 5(b), bottom left]. However, since both Bond numbers were changed simultaneously, two additional simulations are

needed to decouple the effects of Bo^- and Bo^+ and determine which dominates the jetting process.

We again begin with our nondroplet producing case [Fig. 5(b), top right]. However, instead of keeping the influence of gravity constant, we decrease the Bond number used for calculating the evolution of the jet to 0.01 ($Bo^+ = 0.01$) the instant the simulation starts [Fig. 5(b), top right → top left]. Even with this large reduction in Bo^+, droplets are still not produced. Now, beginning with the droplet producing case [Fig. 5(b), bottom left], we increase the Bond number used for calculating the evolution of the jet to 1.3 ($Bo^+ = 1.3$) as the simulation begins [Fig. 5(b), bottom left → bottom right]. Again, we see that a large change in Bo^+ is insufficient to cause any significant change in the production of jet droplets. In fact, when comparing the two $Bo^+ = 0.01$ cases [Fig. 5(b), left side] with the two $Bo^+ = 1.3$ cases [Fig. 5(b), right side], we see that increasing Bo^+ increases, rather than decreases, the height of the resulting jet. As changes in the surface tension are accounted for by the inertio-capillary time ($\tau = t/\sqrt{\rho_\ell R^3/\gamma}$), the increased jet height at time $\tau = 0.2$ can be attributed to the increase in the hydrostatic (gravitational) pressure. Because the simulations demonstrate that the presence of jet drops depends on the Bond number before rupture (Bo^-), rather than the Bond number after rupture (Bo^+), we believe that the dominant role that gravity has in this jetting process is setting up the initial bubble shape [Fig. 5(a)].

By connecting the viscous and gravitational limits on jet-drop formation, we reveal the existence of an intermediate regime. We expect to encounter this phenomenon in a variety of applications ranging from metalworking fluid [39] to sea slicks, both natural [40,41] and anthropogenic [42]. Further, through simulation we show how the existence of this region can be rationalized as a coupling between the equilibrium bubble shape and viscous effects.

The authors thank E. Lewis for helpful discussions. The authors also acknowledge support from the National Science Foundation under Grant No. 1351466 and from the École Polytechnique internship program.

[1] D. Blanchard and L. Syzdek, Science **170**, 626 (1970).
[2] D. Blanchard and L. Syzdek, J. Geophys. Res. **77**, 5087 (1972).
[3] E. Baylor, V. Peters, and M. Baylor, Science **197**, 763 (1977).
[4] E. Baylor, M. Baylor, D. Blanchard, L. Syzdek, and C. Appel, Science **198**, 575 (1977).
[5] B. C. Parker, M. A. Ford, H. Gruft, and J. O. Falkinham 3rd, Am. Rev. Respir. Dis. **128**, 652 (1983).
[6] A. H. Woodcock, J. Mar. Res. **7**, 56 (1948).
[7] S. G. Boyce, Science **113**, 620 (1951).
[8] C. Kientzler, A. Arons, D. Blanchard, and A. Woodcock, Tellus **6**, 1 (1954).
[9] D. C. Blanchard, Prog. Oceanogr. **1**, 73 (1963).
[10] E. R. Lewis and S. E. Schwartz, *Sea Salt Aerosol Production: Mechanisms, Methods, Measurements and Models—A Critical Review* (American Geophysical Union, Washington, DC, 2004), Vol. 152.
[11] F. MacIntyre, J. Geophys. Res. **77**, 5211 (1972).
[12] I. J. Bear and R. G. Thomas, Nature (London) **201**, 993 (1964).
[13] Y. S. Joung and C. R. Buie, Nat. Commun. **6**, 1 (2015).
[14] D. C. Blanchard and L. D. Syzdek, J. Geophys. Res.: Oceans **93**, 3649 (1988).
[15] D. E. Spiel, J. Geophys. Res.: Oceans **103**, 24907 (1998).
[16] H. Lhuissier and E. Villermaux, J. Fluid Mech. **696**, 5 (2012).
[17] F. Knelman, N. Dombrowski, and D. M. Newitt, Nature (London) **173**, 261 (1954).
[18] O. Stuhlman, J. Appl. Phys. **2**, 457 (1932).
[19] L. Duchemin, S. Popinet, C. Josserand, and S. Zaleski, Phys. Fluids **14**, 3000 (2002).
[20] E. Ghabache, A. Antkowiak, C. Josserand, and T. Séon, Phys. Fluids **26**, 121701 (2014).
[21] D. C. Blanchard, Nature (London) **173**, 1048 (1954).
[22] D. Blanchard, J. Geophys. Res. **94**, 10999 (1989).
[23] D. E. Spiel, J. Geophys. Res. **99**, 10289 (1994).
[24] B. W. Zeff, B. Kleber, J. Fineberg, and D. P. Lathrop, Nature (London) **403**, 401 (2000).
[25] See Supplemental Material at http://link.aps.org/supplemental/10.1103/PhysRevE.92.021002 for high-speed videos of the experiments shown in Fig. 1.
[26] J. S. Lee, B. M. Weon, S. J. Park, J. H. Je, K. Fezzaa, and W.-K. Lee, Nat. Commun. **2**, 367 (2011).
[27] S.-C. Georgescu, J.-L. Achard, and E. Canot, Eur. J. Mech. B: Fluids **21**, 265 (2002).
[28] J. G. Woodward, J. Acoust. Soc. Am. **25**, 147 (1953).
[29] C. E. Stauffer, J. Phys. Chem. **69**, 1933 (1965).
[30] Glycerine Producers' Association *et al.*, *Physical Properties of Glycerine and Its Solutions* (Glycerine Producers' Association, New York, NY, 1963).
[31] R. Scardovelli and S. Zaleski, Annu. Rev. Fluid Mech. **31**, 567 (1999).
[32] P. L. L. Walls, J. C. Bird, and L. Bourouiba, Integr. Comp. Biol. **54**, 1014 (2014).
[33] S. Popinet, J. Comput. Phys. **190**, 572 (2003).
[34] S. Popinet, J. Comput. Phys. **228**, 5838 (2009).
[35] D. Fuster, G. Agbaglah, C. Josserand, S. Popinet, and S. Zaleski, Fluid. Dyn. Res. **41**, 065001 (2009).
[36] G. Agbaglah, S. Delaux, D. Fuster, J. Hoepffner, C. Josserand, S. Popinet, P. Ray, R. Scardovelli, and S. Zaleski, C. R. Mecanique **339**, 194 (2011).
[37] M. K. Tripathi, K. C. Sahu, and R. Govindarajan, Nat. Commun. **6**, 6268 (2015).
[38] Y. Toba, J. Oceanogr. Soc. Jpn. **15**, 121 (1959).
[39] D. I. Bernstein, Z. L. Lummus, G. Santilli, J. Siskosky, and I. L. Bernstein, Chest **108**, 636 (1995).
[40] D. J. Carlson, Nature (London) **329**, 823 (1987).
[41] L. Seuront, D. Vincent, and J. G. Mitchell, J. Marine Syst. **61**, 118 (2006).
[42] S. D. Asl, J. Amos, P. Woods, O. Garcia-Pineda, and I. R. MacDonald, Deep-Sea Res., Pt. II (2014).